LBL--31666

DE93 007659

Radioelements and Their Occurrence with Secondary Minerals in Heated and Unheated Tuff at the Nevada Test Site

S. Flexser and H.A. Wollenberg

Earth Sciences Division
Lawrence Berkeley Laboratory
University of California
Berkeley, California 94720

June 1992

This work was supported by the Director, Office of Civilian Radioactive Waste Management, Office of Facilities Siting and Development, Siting and Facilities Technology Division, of the U.S. Department of Energy under Contract No. DE-AC03-76SF00098.

ABSTRACT

Samples of devitrified welded tuff near and away from the site of a heater test in Rainier Mesa were examined with regard to whole-rock radioelement abundances, microscopic distribution of U, and oxygen isotope ratios. Whole-rock U averages between 4 and 5 ppm, and U is concentrated at higher levels in primary and secondary opaque minerals as well as in accessory grains. U in secondary sites is most commonly associated with Mn phases, which average ~30 ppm U in more uraniferous occurrences. This average is consistent and apparently unaffected by proximity to the heater. The Mn phases differ compositionally from Mn minerals in other NTS tuffs, usually containing abundant Fe, Ti, and sometimes Ce, and are often poorly crystalline. Oxygen isotope ratios show some depletion in $\delta^{18}O$ in tuff samples very close to the heater; this depletion is consistent with isotopic exchange between the tuff and interstitial water, but it may also reflect original heterogeneity in isotopic ratios of the tuff unrelated to the heater test. Seismic properties of several tuff samples were measured. Significant differences correlating with distance from the heater occur in P- and S-wave amplitudes; these may be due to loss of bound water. Seismic velocities are nearly constant and indicate a lack of significant microcracking. The absence of clearer signs of heater-induced U mobilization or isotopic variations may be due to the short duration of the heater test, and to insufficient definition of pre-heater-test heterogeneities in the tuff.

INTRODUCTION

Understanding the chemical and physical effects of heating on repository rock is important for predicting the behavior of the rock medium after emplacement of high-level waste. In this study, we examined rock from the vicinity of a prototype heater test, conducted by Lawrence Livermore National Laboratory in the unsaturated zone in G-tunnel, Rainier Mesa, Nevada Test Site (NTS), that simulated the thermal effects of waste emplacement. By the close of the test, which lasted approximately 6 months, the temperature at the heater edge reached 240 °C, with a zone of dried rock surrounding the heater. A detailed description of the heater experiment and the perturbations of temperature and moisture content in surrounding rock are provided by Ramirez et al. (1990). The host rock for the heater test was densely welded and devitrified tuff of the Grouse Canyon Member of the Belted Range Tuff, and is similar in its mineralogy and thermomechanical properties to the welded Topopah Spring Member of the Paintbrush Tuff (Connolly et al., 1983), the potential Yucca Mountain repository medium.

In this report, we examine effects on the tuff of heating and interaction with hot water and steam. These effects include possible mobilization of uranium,

and changes in oxygen isotope ratios and seismic properties of the tuff. We focus on the distribution of U, especially in secondary sites from which U is most prone to mobilization, and which preserve a record of U migration earlier in the history of the tuff. There is significant alteration of mafic and opaque phenocrysts in the tuff, with secondary deposition of Fe- and especially Mn-rich phases. The abundance of secondary Mn minerals in the tuff, and their association with elevated levels of U, is of particular interest as a number of common Mn-oxide minerals are potentially important for waste isolation due to their open tunnel-like structures and capacity for sorption of actinide elements (Means et al., 1978). Manganese minerals are present as well in the Topopah Spring welded tuff and underlying Calico Hills and Crater Flat tuffs (Carlos, 1985, 1987; Carlos et al., 1990), and we have therefore attempted to characterize the Mn minerals' occurrence and composition in the Grouse Canyon tuff as well as any effects due to proximity to the heater.

METHODOLOGY

The distribution of uranium was determined on both macroscopic and microscopic scales. Whole-rock concentrations of U, Th, and K were determined by γ-spectrometry from the γ-ray peaks of ^{214}Bi, ^{208}Tl, and ^{40}K, respectively. One sample was also analysed by high-resolution γ-spectrometry for evidence of disequilibrium among the U-series daughter nuclides ^{234}Th, ^{234}Pa, ^{226}Ra, ^{214}Pb, and ^{214}Bi. On the microscopic scale, fission-track radiographs of polished thin sections were prepared by irradiation with a thermal neutron flux of 3.6×10^{14} neutrons/cm^2 to discern U concentrations. Radiographs were studied in conjunction with mineralogical observation in the petrographic microscope, and U concentrations were determined by counting associated fission tracks and calibrating track densities with those of standard glasses (also exposed to the same neutron flux) containing 43 ppm U. The error in this method is probably under ±10% in the best case of large mineral grains of simple cross-sectional geometry and U concentrations greater than ~10 ppm. Larger errors apply to track counts of irregular or intergrown minerals such as the Mn phases abundant in the groundmass of the tuff. Sites of U concentration and secondary mineralization were also examined in the scanning electron microscope (SEM), with the back-scattered electron (BSE) mode especially useful for imaging opaque minerals finely intergrown with the tuff groundmass. Compositional data were obtained with the SEM by analysis

of energy-dispersive x-ray spectra (EDS) employing a standardless matrix correction (atomic number absorption fluorescence, or ZAF), and were semiquantitative. Several samples were also examined in an analytical transmission electron microscope (ATEM) to obtain compositional and crystallographic data using a very narrow electron beam.

DISTRIBUTION OF URANIUM IN THE TUFF

Core samples of the welded tuff were obtained from a 12-inch-diameter borehole (P-1) that was drilled back through the heated rock following completion and cool-down of the heater experiment (Fig. 1). Sample locations ranged from centimeters to >6 m from the heater edge. Samples of unheated core were also obtained from a borehole (NE-2) which was drilled prior to the heater test, and which approached to within 1 m of the location of the heater. Figure 2, taken from Ramirez et al. (1990), illustrates the scale of interaction of the heater with the tuff, and the effects of the heater on moisture distribution in adjacent tuff at the close of the heater experiment, while maximum temperatures reached are shown in Figure 3D. Figure 2 depicts the dried zone extending from the heater ~0.7 m radially into the tuff, surrounded by a condensation annulus from which water flowed outward, as well as backwards toward the heater following heater turn-off. Steam and, initially, water also flowed into the heater hole before drying.

Whole-rock U, Th, and K concentrations in heated tuff between 3 and 300 cm from the heater are shown in Figure 3, along with mean U, Th, and K of 9 samples of unheated tuff from between ~50 and ~650 cm from the heater position (see Appendix A). (These γ-spectrometric data are uncorrected for radon emanation, which in two samples was measured at ~15%. As Rn emanation is likely to be similar in the other samples, actual U concentrations would be ~15% higher than the reported values in all cases.) From the figure, it can be seen that both U and Th concentrations in samples farther than 30 cm from the heater are high relative to samples closer to the heater, as well as to unheated samples. This suggests that there may be a relation between radioelement abundances and effects of the heater on the rock and on fluid movement, as sketched in Figure 2. On the other hand, the similar trends of Th and U suggest that primary compositional variability in the tuff, beyond that reflected in the 9 unheated samples, may be the more probable explanation, as Th is unlikely to be as mobile as U during fluid mobilization caused by heating.

The fact that K matches Th very closely in the heated tuff also tends to support this latter interpretation. It is thus unclear from the whole-rock data alone whether the distribution of radioelement contents reflects changes caused by the heater experiment, and a more detailed fission-track microscopic study of U loci in the tuff was undertaken to address this question.

In the tuff groundmass, U is distributed rather uniformly between 2 and 3 ppm, compared with 4 to 5 ppm whole-rock levels. U occurs at much higher concentrations in opaque primary and secondary minerals, as well as in primary accessory minerals. The accessory minerals, mainly zircon with lesser monazite, contain the highest U concentrations in the tuff, commonly several hundred ppm or more, but they are largely unaltered (with the exception of a sparse Ti-Ce silicate mineral), and their contained U is probably not liable to mobilization by hot water. In primary opaque minerals, U is present mainly in magnetite (typically 30 to 80 ppm U), while it is nearly absent from ilmenite and titanomagnetite.

The most abundant U-bearing opaques, which we focus on here, are Mn-rich phases which appear in hand-specimen as dark brown stains in the tuff groundmass. Microscopically, these are seen to be irregular clusters, either dense or diffuse, which often include or are connected by very fine fractures (Fig. 4). The concentrations of U associated with these sites vary widely between groundmass levels and tens of parts per million, with most containing between 15 and 40 ppm.

Alteration products of mafic phenocrysts or phenocryst clusters comprise another category of U-bearing secondary opaques, with U concentrations typically in the range of 30 to 100 ppm. These are typically composite intergrowths of fine-grained magnetite and other Fe-, Mn-, and Ti-oxides, with inclusions of silicates, apatite, and monazite. Figure 5 is an example of this type of opaque (its composite nature is obscured by the brightness of the BSE image), with later opaque alteration adjacent to it and trailing into the groundmass. Similar alteration haloes or tails are common around primary opaque and altered mafic grains; they are not generally distinguishable in texture or composition from the above-described Mn-rich groundmass clusters, except that high concentrations of Fe are often observed within 10 - 20 μm of the grains, which drop off sharply beyond that. Pseudomorphic coatings of fayalite are another common, though much less abundant type of U-bearing

mafic replacement. The Fe-rich coatings usually contain between 30 and 70 ppm U, with little or no detectable U associated with the remnant fayalite.

Table 1 summarizes the fission-track data on U concentrations associated with opaques in the heated tuff. The whole-rock U data of Figure 3 are also shown for comparison. The data on the opaque minerals are representative samplings rather than true averages, as suggested by the number of sites counted and the high standard deviations. Although the data on the secondary Mn clusters appear uniform relative to other opaques, this is somewhat deceptive as there can be large errors in estimating their U concentrations due to the irregular intergrowth of the clusters with the groundmass. Also, the difficulty in determining low concentrations of U by the fission-track method means that the U data on these secondary sites are weighted somewhat toward the upper range of U contents. The data in Table 1 are plotted in Figure 6, with primary opaques and replaced-mafic grains grouped together for simplicity. The secondary Mn clusters show fairly uniform U concentrations without apparent effect of proximity to the heater, although changes in U content in less-uraniferous Mn clusters could remain undetected. Other opaques plotted in Figure 6A show greater variation in U concentrations, but that variation is not large given the very high standard deviations of much of that data.

At 300 cm from the heater, anomalously high U is characteristic of all types of opaques. The whole-rock data for this sample also show high U abundance. This anomaly is unlikely to be related to the heater test, both because of the distance of this sample from the heater, and because primary as well as secondary opaques show high U contents that are distributed uniformly rather that preferentially at grain margins. We also investigated U-series disequilibrium in this sample by means of whole-rock high-resolution γ-spectrometry. Examination of the γ-ray peaks from ^{234}Th, ^{234}Pa, ^{226}Ra, ^{214}Pb, and ^{214}Bi did not show evidence for disequilibrium, and indicated that the anomalous U concentrations in this sample either reflect primary composition or secondary redistribution that occurred in response to fluid circulation in the cooling tuff sheet soon after its deposition.

SECONDARY MANGANESE MINERALS

The most common sites of secondary U in the tuff are Mn phases, which occur as irregular clusters in the groundmass (Fig. 4) or as alteration haloes around primary opaque or replaced-mafic grains (Fig. 5), and with U

concentrations as shown in Figure 6. The Mn phases are tightly interwoven with collapsed pumice comprising most of the groundmass, and in cross-section they appear as sieve-textured clusters of micron-sized irregular or dendritic lobes. They also occur commonly in very fine fractures in and between the clusters, which in most cases are probably interconnected by such fractures outside the plane of the thin sections. The examples shown in Figure 7 - similar to Figure 4, but employing BSE images - illustrate these typical textures of the Mn minerals, as well as the welded pumice texture and micro-porosity of the groundmass. The Mn minerals are often mixed with fine hematite or other Fe-oxide phases; this is observed immediately adjacent to primary or replaced-mafic opaques, and to a lesser degree throughout the groundmass which is extensively stained by disseminated hematite.

SEM analyses by EDS indicate that the secondary Mn clusters are complex and variable in composition, although analyses of pure phases are difficult to obtain due to their finely intergrown nature. Table 2 is a compilation from different sites of representative high-Mn EDS analyses. Several representative SEM spectra and EDS analyses are also given in Appendix B, and show similar compositions to those in Table 2. Columns A and B in Table 2 are two possibly distinct groups of analyses of the common groundmass clusters, and they show abundant and variable FeO and often TiO_2 included with MnO. In an attempt to determine compositions of distinct phases, a small number of samples were studied in the analytical transmission electron microscope (ATEM), which employs an extremely narrow beam (~150 Å). Column C in Table 2 averages several consistent analyses within one secondary cluster, and it is quite different from the SEM analyses, with much higher Fe and Ti, and lower Ca. This is also illustrated in Figure 8, which represents graphically the data of Table 2. X-ray diffraction by TEM reveals that the material comprising the analyses in column C is largely amorphous, with degree of crystallinity roughly correlating with higher Mn and lower Si contents. It is not clear whether the compositions shown in columns A, B, and C represent discrete phases, or consistent mixtures intergrown on a sub-micron scale. Intergrowth with hematite could account for the differences in Fe concentrations, and possibly also in Ti, which varies sympathetically with Fe in these analyses and is often abundant in groundmass hematite. Micron- and sub-micron-size discrete grains of rutile or anatase are also common in the groundmass, and could be intermixed as well.

Cerium is commonly present in the Mn-rich clusters at concentrations of several percent CeO_2, and in a number of analyses >10% CeO_2. (Given the problems of overlap between x-ray peaks of Ti, Ce, and Ba, Ce peak positions were checked closely against those of Ti and Ba. Appreciable Ba was not observed in the groundmass clusters. Analyses in Table 2 are normalized to zero concentration of CeO_2 and other non-tabulated oxides.) Up to 1 to 2% ZrO_2, and possibly some P, are also associated. The presence of Ce may have implications for the distribution of Th in the tuff, as Ce and Th can follow similar geochemical paths in weathering processes (eg., Lei et al., 1986). In addition to secondary opaques, Ce is present in a primary accessory mineral which, unlike other accesories, shows significant alteration. The mineral occurs as sparse elongate pleochroic prisms with the approximate composition SiO_2: 35%, TiO_2: 27%, FeO: 16%, CeO_2: 14%, CaO: 5% (carbonate not determined). Altered portions consist of distinct TiO_2 and Ce-silicate phases. Approximately 80 ppm U is present in the unaltered mineral, with much higher concentrations associated with the alteration products. Given the alteration of this mineral, and the evidence for adjacent redistribution of Ce, it appears to be one likely source of mobile Ce for deposition in Mn-rich secondary sites.

Secondary Mn phases of different morphologies than the groundmass clusters exemplified in Figures 4 and 7 are present but much less common in the tuff. In one sample, from a localized zone with abundant secondary Mn as well as dark disseminated-hematite staining, Mn phases occur in pores 100 to 200 μm in diameter as dense linings and late-stage fine acicular crystals (Fig. 9), analyses of which are shown in Table 2 (cols. D - F) and are plotted in ternary diagrams in Figure 8. These analyses form a much tighter set than those of the groundmass clusters, although they also include abundant Fe and Ti. The ATEM analyses (Table 2, col. F) show greater variability than the SEM data, and indicate that amorphous material is intermixed in these phases also, despite their euhedral morphology. Their U concentrations are similar to that of the groundmass and well below those of the common Mn clusters, and their Ce contents are also low.

Higher Mn concentrations in secondary sites were also observed very locally in the tuff in relatively thick fracture and pore fillings (Fig. 10), fillings in biotite cleavages, and sometimes adjacent groundmass clusters. Analyses of these Mn minerals (Table 2, col. G, and Fig. 8) show that the high Mn contents are offset by lower Ti, and especially Fe, than in other secondary Mn sites. K is also

significantly higher, and small amounts of Pb and possibly Ba are sometimes present as well, suggesting that this is a mineral of the cryptomelane-hollandite-coronadite group. Concentrations of ~30-40 ppm U are often associated with these Mn minerals, and Ce is generally sparse or absent.

Most Mn phases in the Grouse Canyon tuff differ in composition, especially with respect to abundance of Fe and Ti, from Mn minerals in tuffs elsewhere at the NTS. In the Crater Flat Tuff, Mn minerals are mainly of the cryptomelane-hollandite group (Carlos, 1987; Carlos et al., 1990). In two samples of devitrified Topopah Spring welded tuff examined in this study, Mn minerals are less abundant than in the Grouse Canyon, and confined to fine fractures. They typically contain Pb and Ba (probably cryptomelane-hollandite), along with substantial Al (lithiophorite), in agreement with observations of Carlos (1987). They also show no clear association with U above groundmass levels.

Textural and compositional evidence from secondary sites points to a complex relationship of solution and deposition between Fe and Mn in the tuff. The high Fe contents in most Mn-rich groundmass clusters (Table 2, cols. A - C) are probably often related to incorporation of earlier-deposited disseminated hematite or other Fe-oxides, while co-deposition of Fe and Mn probably occurred in the acicular cystals and linings in the larger pores (Table 2, cols. D - F). Where alteration is present adjacent to primary or replaced-mafic opaques, Fe was deposited quickly while Mn was more stable in solution and carried much farther from the grains. In still other cases, hematite appears to have been reduced and dissolved while Mn was precipitated from solution, in much the same way as reduction of many Mn minerals can immobilize other oxidizable cations such as actinides (Carlos et al., 1990). This is indicated, in a number of samples in which hematite staining is abundant, by the marked absence of such staining within haloes surrounding all secondary Mn clusters. The variety of modes of behavior of Fe and Mn during solution and deposition (with more than one type often observed in a single sample) suggests that deposition of the Mn minerals in the tuff was probably a complex process involving different generations of fluids. It appears to be unrelated to short-term heater effects, and probably occurred not long after eruption, during circulation of fluids in the cooling ash-flow sheet.

OXYGEN ISOTOPES

Two sets of oxygen isotope analyses of samples of the tuff were obtained to determine whether there were any discernible effects on isotope ratios caused by the heater test and the consequent interaction with the tuff of hot water and steam. Samples were prepared that were representative of groundmass material, relatively free of large phenocrysts, fiamme, or lithic inclusions. The first set of analyses included 9 samples of the drillback (P-1) core, ranging from 3 to 300 cm from the edge of the heater hole, and the results from this set (Appendix C) are shown in Figure 11 by the dashed line. Low values of $\delta^{18}O$ are seen in close proximity to the heater hole where temperatures were near 200 °C, relatively high values at 20-100 cm, then lower ratios at 160 and 300 cm. The steep gradient in $\delta^{18}O$ over the first 20 cm suggests significant interaction between the tuff and water or steam in this zone of heating, similar on a very small scale to the variation of $\delta^{18}O$ and temperature in rock encompassed by an active hydrothermal system.

To estimate the amount of water that could have interacted with the tuff to produce this apparent $\delta^{18}O$ anomaly adjacent to the heater, we first used an equation relating the difference in $\delta^{18}O$ between water and a coexisting mineral phase to the temperature (°K) at which the mineral equlibrated oxygen with the water (Faure,1986):

$$\Delta = \delta_m - \delta_w = A(10^6 T^{-2}) - B \qquad (1)$$

where δ_m and δ_w are $\delta^{18}O$ values for the mineral and water, respectively, and A and B are constants that depend on the mineral. The Δ value from (1) was then entered into an equation relating ratios of exchangeable molar amounts of oxygen in water and rock (W/R) to their isotopic compositions (Henley et al.,1984):

$$W/R = (\delta_{f,\,rock} - \delta_{i,rock}) / \delta_{i,water} - (\delta_{f,rock} - \Delta) \qquad (2)$$

where δ_i and δ_f are initial and final isotopic ratios, respectively. We used $\delta_{f,rock}$= 8.3, $\delta_{i,rock}$ = 9, $\delta_{i,water}$ = -13 (from Russell et al., 1988, for water in Rainier Mesa tuff), and T=200 °C for conditions adjacent to the heater. Using a quartz-feldspar mineralogy to represent the tuff, and substituting the appropriate values of A and B for these minerals in eqn. (1) yields Δ between 9.6 (feldspar) and 11.7 (quartz), and (2) yields a molar water-rock ratio between 0.061 and 0.075. Accounting for the difference in oxygen content between water and the Grouse

Canyon tuff (from Connolly et al., 1983) results in a water/rock mass ratio of 0.031 to 0.038 or, at a rock density of 2.5, a volume ratio of 0.08 to 0.1. This is quite comparable to the volume ratio of interstitial water to rock, as the average porosity of the tuff is ~0.1 (L.R. Myer, pers. comm.), and saturation in the tuff ranges from 60 to 100% (Russell et al., 1988).

Isotopic exchange between the tuff and interstitial pore water could therefore reasonably account for the apparent depletion in ^{18}O in rock adjacent to the heater. The above calculation is still but a first approximation, as a number of other factors could have had a large effect on the inferred water-rock ratio. The assumed quartz-feldspar mineralogy, for example, would need revision if there was significant interaction of hot water with non-silicate phases, specifically Mn or Fe minerals, for which the oxygen exchange behavior (the values of A and B in eqn. 1) can be quite different from that of silicates. Also, more-complex water-rock interactions than simple exchange between rock and pore water may well have played a role, given the complicated effects of heating, presence of a vapor phase, drying, partial re-wetting of the tuff following heater turn-off, and fracture flow, sketched in Figure 2 and described by Ramirez et al. (1990).

In order to better determine the "baseline" variability of oxygen isotope ratios in the tuff prior to introduction of the heater, and to verify whether the low ratios very close to the heater are indeed anomalous, analyses were obtained of a second set of samples of the tuff. These included duplicate samples from 3.5 cm and 24 cm from the heater edge, another sample of the drillback core from 640 cm, and two samples of unheated NE-2 core (Appendix C). The data from this sample set are also plotted in Figure 11, and though they show good agreement in several cases with the first set, there is a significant discrepancy for the sample closest to the heater. This fact, as well as the larger "baseline" variability implied by the sample of unheated core at ~190 cm, casts some doubt on the anomaly very close to the heater that was suggested by the first set of isotope analyses. The anomaly and the amount of water-rock interaction needed to account for it is probably smaller than that originally inferred, and it remains somewhat ambiguous to what degree the observed variation in oxygen isotope ratios is due to heater-induced effects as opposed to pre-heating heterogeneity in the tuff.

SEISMIC PROPERTIES

Another approach toward detecting effects on the tuff of proximity to the heater was the determination of seismic properties of 3 sub-cores drilled from the heated P-1 core. The dimensions of the sub-cores were 3.8 cm in length and 5.1 cm in diameter, and they were centered at approximately 3.5, 17, and 30 cm from the edge of the heater hole (Appendix D). The seismic velocities of the three samples were very similar: the variation in compressional (P) and shear (S) wave velocities and in the velocity ratio were only 2.9%, 4.6%, and 1.6%, respectively, while the variation in density of the core samples was 3.2%. The lack of variation in seismic velocities is a strong indication that micro-cracking was not a factor even in tuff very close to the heater.

A marked difference was observed, however, with regard to seismic amplitudes of the core samples, which were measured over a range of axial stresses as shown in Figure 12. Amplitudes of both P- and S-waves increased with proximity to the heater, although for P-waves the increase was confined to the closest sample. The increase in amplitudes adjacent to the heater could be related to loss of bound water either from fine crack terminations and asperities, or from clay minerals such as smectite, which is common in some pumice inclusions but otherwise a minor component of the tuff. The water loss could have been small enough to have no measurable effect on the stiffness (and hence velocity) of the rock, but large enough to affect the seismic energy loss, and resultant amplitude attenuation, caused by interaction with water (L.R. Myer, pers. comm.). Further tests on these and other samples, including laboratory drying at heater-test temperatures, would be useful in testing the validity of this interpretation.

CONCLUSIONS

Detailed examination of uranium concentrations in primary and secondary opaques in the Grouse Canyon welded tuff, at varying distances from the heater, disclosed no definitive effects on U distribution of heating and interaction with hot water. Whole-rock U abundances also showed no apparent changes correlating with distance from the heater. Oxygen isotope ratios in an interval of the tuff very close to the heater edge are somewhat anomalous and may indicate exchange between tuff and hot water or steam, but the anomalous ratios do not fall distinctly outside the range of pre-heater-test variation in the tuff. One case in which effects of the heater test were clearly observed was the

variation of amplitudes of seismic waves propagating through the tuff, which may reflect loss of bound water very close to the heater. Seismic velocities were nearly constant, however, indicating a lack of significant microcrack development adjacent to the heater.

This study also documented the association of U with secondary opaque sites in the tuff, particularly Mn-rich opaques commonly intergrown with the groundmass. These typically contain abundant Fe, Ti, and sometimes Ce, are often poorly crystalline, and span a wide range of U concentrations. Their compositions generally differ from those of Mn minerals in other tuffs at the NTS. The affinity of Mn phases for U in the Grouse Canyon tuff underlines the need to give careful consideration to Mn phases in assessing the potential of a rock to retard the migration of U.

The absence of unambiguous effects of the heater on most of the parameters investigated in this study may reflect the short time span of the heater test. Changes in U distribution may be present but too minor to distinguish via fission tracks from groundmass "background" U or from the relatively high U contained in some opaque minerals, and variations in isotope ratios may reflect only the early stages in the formation of a well-defined heater-induced anomaly. This points up the need, if future *in situ* heater experiments are undertaken, for a longer time scale, and for more-detailed initial sampling to better define "baseline" heterogeneity in rock composition for later comparison with possible effects of heating. Sampling of pore water before and after heating, and collection of water flowing into the heater hole, would also be valuable for a comprehensive interpretation of the fluid-rock interaction.

ACKNOWLEDGMENTS

We would like to thank Alan R. Smith for γ-spectrometric analyses of radioelement concentrations, Gee-Minn Chang, Dan Schrag, and Brian Smith for oxygen isotope analyses, and Larry Myer and Curt Nehay for measurements of seismic properties. We also appreciate the help of Ron Wilson, with the Department of Material Science and Mineral Engineering, U. C. Berkeley, with scanning electron microscopy; the Oregon State University Radiation Center for thermal neutron irradiations; Chuck Echer with analytical transmission electron microscopy; and Abelardo Ramirez and William Glassley of Lawrence Livermore National Laboratory in obtaining core samples for this study. This work was sponsored by the Director, Office of Civilian Radioactive Waste

Management, Office of Facilities Siting and Development, Siting and Facilities Technology Division of the U.S. Department of Energy under Contract No. DE-AC03-76SF00098.

REFERENCES

Carlos, B.A., 1987. Minerals in fractures of the saturated zone from drill core USW G-4, Yucca Mountain, Nye County, Nevada. Los Alamos National Laboratory report LA-10927-MS.

Carlos, B.A., 1985. Minerals in fractures of the unsaturated zone from drill core USW G-4, Yucca Mountain, Nye County, Nevada. Los Alamos National Laboratory report LA-10415-MS.

Carlos, B.A., Bish, D.L., and Chipera, S.J., 1990. Manganese-oxide minerals in fractures of the Crater Flat tuff in drill core USW G-4, Yucca Mountain, Nevada. Los Alamos National Laboratory report LA-11787-MS.

Connolly, J.R., Mansker, W.L., Hicks, R., Allen, C.C., Husler, J., Keil, K., and Lappin, A.R., 1983. Petrology and geochemistry of the Grouse Canyon member of the Belted Range tuff, Rock Mechanics drift, U12 G tunnel, Nevada Test Site. Sandia National Laboratories report, SAND 81-1970.

Faure, G., 1986. *Principles of Isotope Geology*, 2nd edition. John Wiley & Sons, New York.

Henley, R.W., Truesdell, A.H., and Barton, P.B., 1984. Fluid-mineral equilibria in hydrothermal systems. Reviews in Economic Geology,1, Society of Economic Geologists.

Lei, W., Linsalata, P., Penna Franca, E., and Eisenbud, M., 1986. Distribution and mobilization of cerium, lanthanum and neodymium in the Morro do Ferro basin, Brazil. Chem. Geol., v. 55, p. 313-322.

Means, J.L., Crerar, D.A., Borcsik, M.P., and Duguid, J.O., 1978. Adsorption of Co and selected actinides by Mn and Fe oxides in soils and sediments. Geochim. Cosmochim. Acta, 42, p. 1763-1773

Ramirez, A.L., Buscheck, T.A., Carlson, R., Daily, W., Latorre, V.R., Lee, K., Lin, W., Mao, N.-H., Towse, D., Ueng T.-S., and Watwood, D., 1990. Prototype heater test of the environment around a simulated waste package. Proc. Internat. Topical Mtg. High Level Waste Mngmnt., Amer. Nucl. Soc., Las Vegas, NV, p.870-881.

Russell, C.E., Hess, J.W., and Tyler, S.W., 1988. Hydrogeologic investigations of flow in fractured tuffs, Rainier Mesa, Nevada Test Site, Desert Research Inst., Water Resources Center pub. 45062.

Distance From Heater (cm)	Secondary Mn-rich clusters (#)	(ppm)	Primary Magnetite Grains (#)	(ppm)	Replaced Mafic Grains (#)	(ppm)	Whole-Rock U (ppm)
1	4	27 (6.3)	1	53	1	33	--
1.8	6	25 (6.3)	3	25 (2)	2	61 (26)	--
3	12	22 (8.2)	6	62 (18)	6	49 (22)	3.33
5.5	5	29 (4.3)	1	42	1	80	--
8	3	29 (8.0)	1	76	3	67 (26)	--
10	10	25 (8.5)	2	52 (27)	3	72 (24)	3.51
17	4	26 (3.9)	1	18	1	73	3.49
24	6	24 (5.6)	3	35 (16)	1	41	3.45
30	6	22 (8.2)	1	61	2	49 (1)	3.38
37	3	25 (5.2)	2	38 (9)		--	4.42
56	5	25 (3.3)	4	40 (12)	3	28 (14)	3.87
163	9	30 (11)	1	35	1	43	4.64
300	10	52 (12)	4	71 (41)	3	194 (31)	5.26
overall	83	28 (12)	30	49 (23)	27	69 (50)	3.93 (.69)

Table 1. Representative U concentrations, determined by fission-track method, of secondary and primary opaque minerals in thin sections, spanning a range of distances from the edge of the heater. Number of sites averaged are shown to left of concentrations; parentheses show standard deviations. Last column is whole-rock U concentrations, by γ-spectrometry, as plotted in Figure 3.

	A (4)	B (7)	*C (4)	D (7)	E (5)	*F (4)	G (4)
MgO				2.2 (1.1)	2.7 (1.)	2.2 (.7)	
Al_2O_3		~2		<0.8	<1		<1
SiO_2	8.6 (4.5)	11.3 (4.0)	22.0 (2.5)	6.5 (2.9)	6.6 (3.8)	2.5 (.3)	2.2 (.1)
K_2O	0.7 (.1)	0.8 (.5)	1.5 (.1)	0.7 (.5)	0.5 (.3)	0.4 (.4)	3.4 (.5)
CaO	5.6 (.4)	5.5 (.9)	2.3 (.6)	3.4 (1.3)	2.6 (.1)	1.6 (.3)	2.6 (.2)
TiO_2	2.5 (.6)	6.4 (3.6)	11.2 (.4)	12.4 (2.6)	7.2 (1.7)	11.3 (4.9)	3.2 (.7)
MnO	70.7 (2.5)	52.1 (6.5)	28.3 (1.8)	52.3 (4.1)	55.3 (3.0)	54.9 (4.9)	83.0 (3.0)
FeO	11.1 (4.1)	19.4 (2.3)	34.0 (.6)	21.9 (2.3)	24.2 (1.4)	27.2 (1.6)	5.0 (1.9)

Table 2. Semiquantitative EDS analyses of Mn-rich secondary sites in the tuff. Analyses performed on scanning electron microscope, or analytical transmission electron microscope (*). Standard deviations given in parentheses. (See Appendix B for several representative x-ray spectra and analyses from columns A - G.)
Common groundmass secondary clusters: A, B, C.
Mn phases in large secondary pores: D (linings), E, F (fine needles).
Thicker high-Mn fillings in fractures and pores: G.

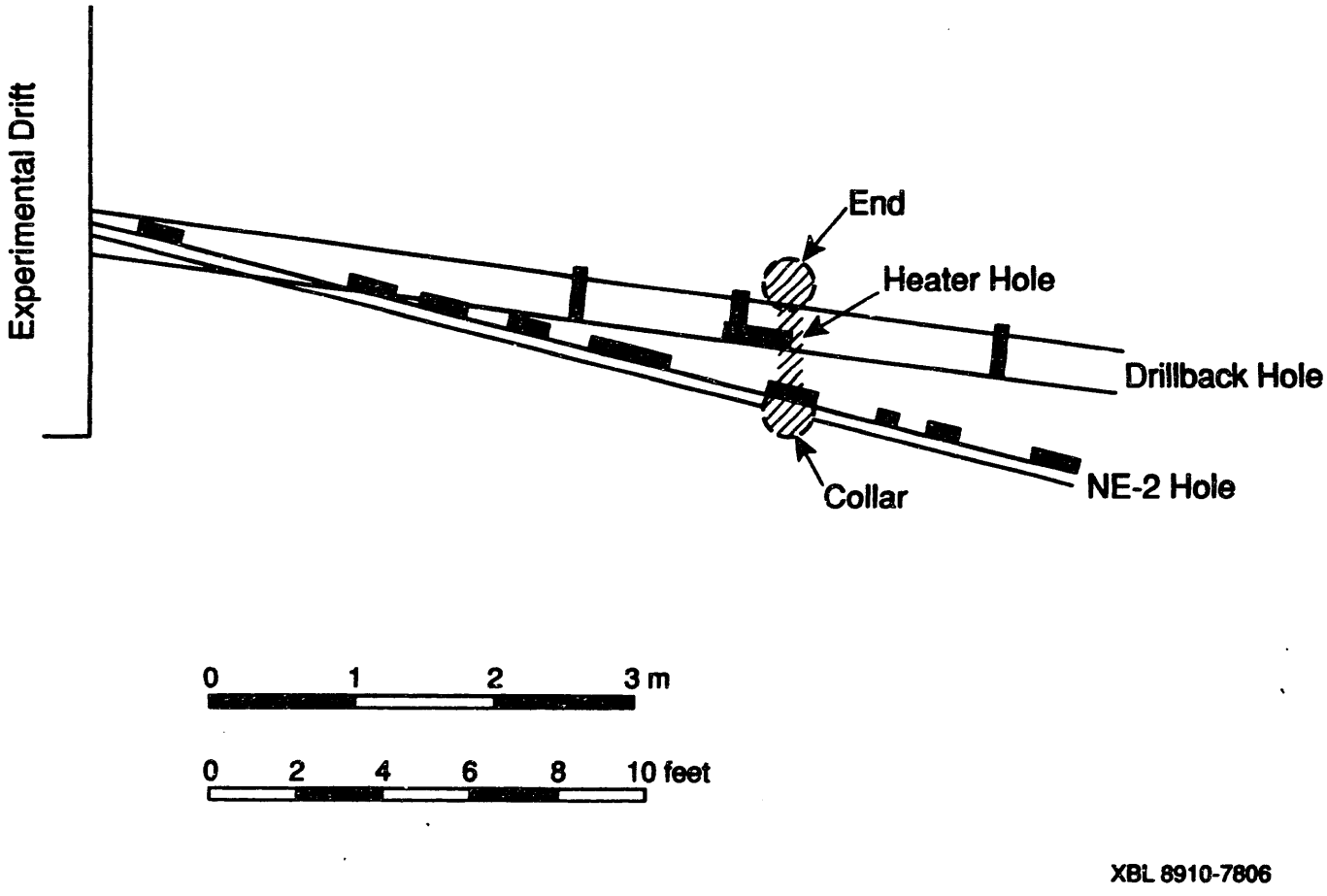

Fig. 1. Vertical section with projections of heater hole and boreholes P-1 (drillback) and NE-2 (drilled prior to the heater hole), at G-tunnel, NTS. The heater is a cylinder 3 m long and 30 cm in diameter, and is tilted ~20° from horizontal.

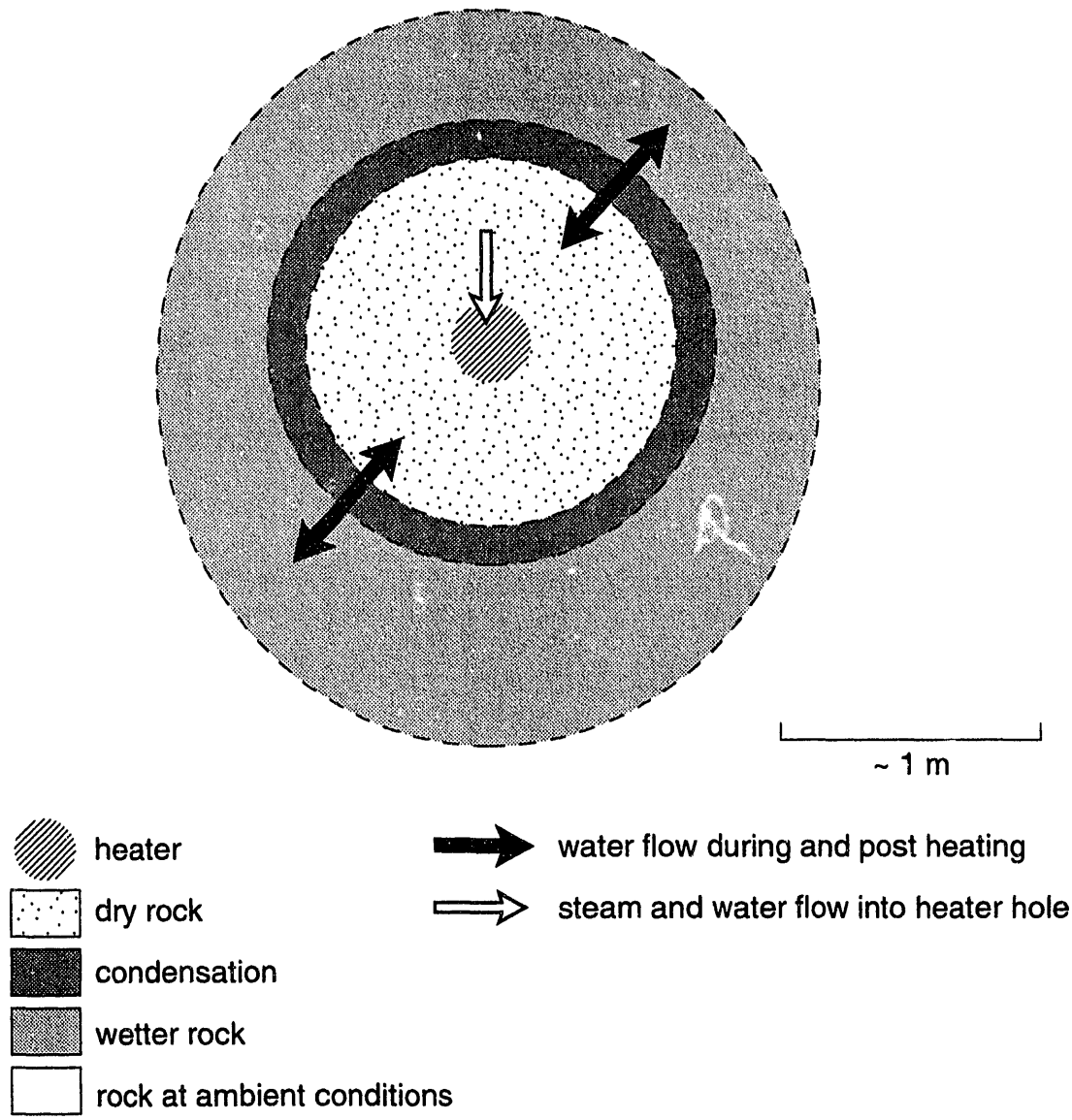

Fig. 2. Conceptual model of moisture distribution and flow, at conclusion of heater test, in tuff surrounding heater. Section is normal to long dimension of heater cylinder. Figure adapted from Ramirez et al. (1990), with fractures ignored for simplicity.

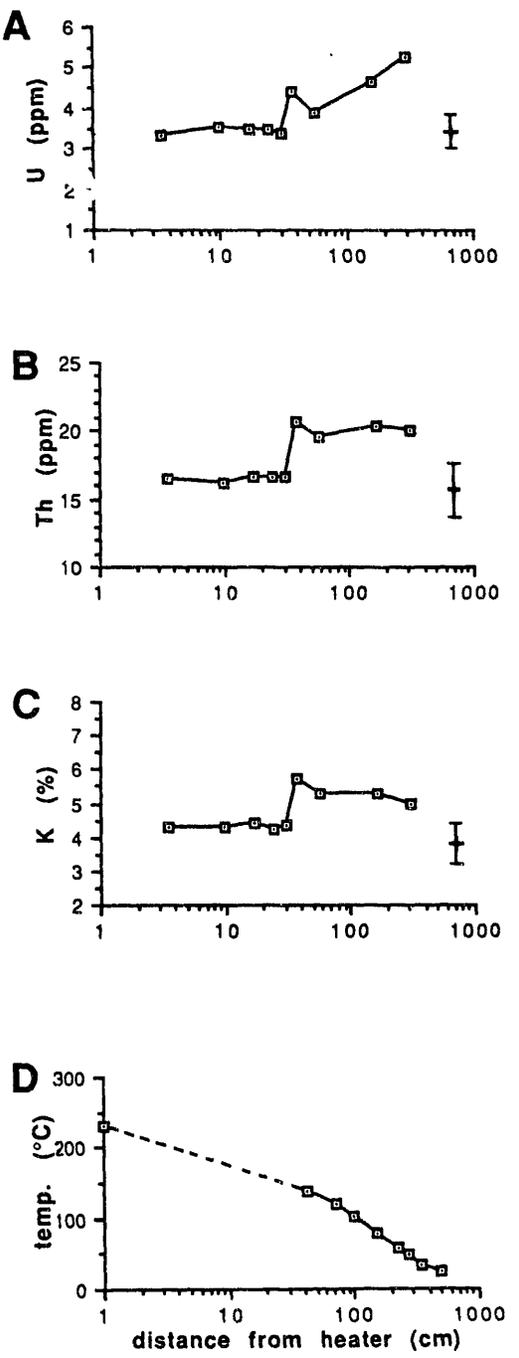

Fig. 3. Whole-rock uranium (A), thorium (B), and potassium (C) abundances in tuff within 300 cm of the heater, plotted against distance from heater edge (log scale). Mean whole-rock U, Th, and K from 9 analyses of unheated tuff from comparable distances from the heater also shown (crosses), with standard deviations (brackets). Maximum rock temperatures during the course of the heater test (after Ramirez et al., 1990) also plotted (D). Radioelement abundances determined by γ-spectrometry. Analyses by A.R. Smith, LBL.

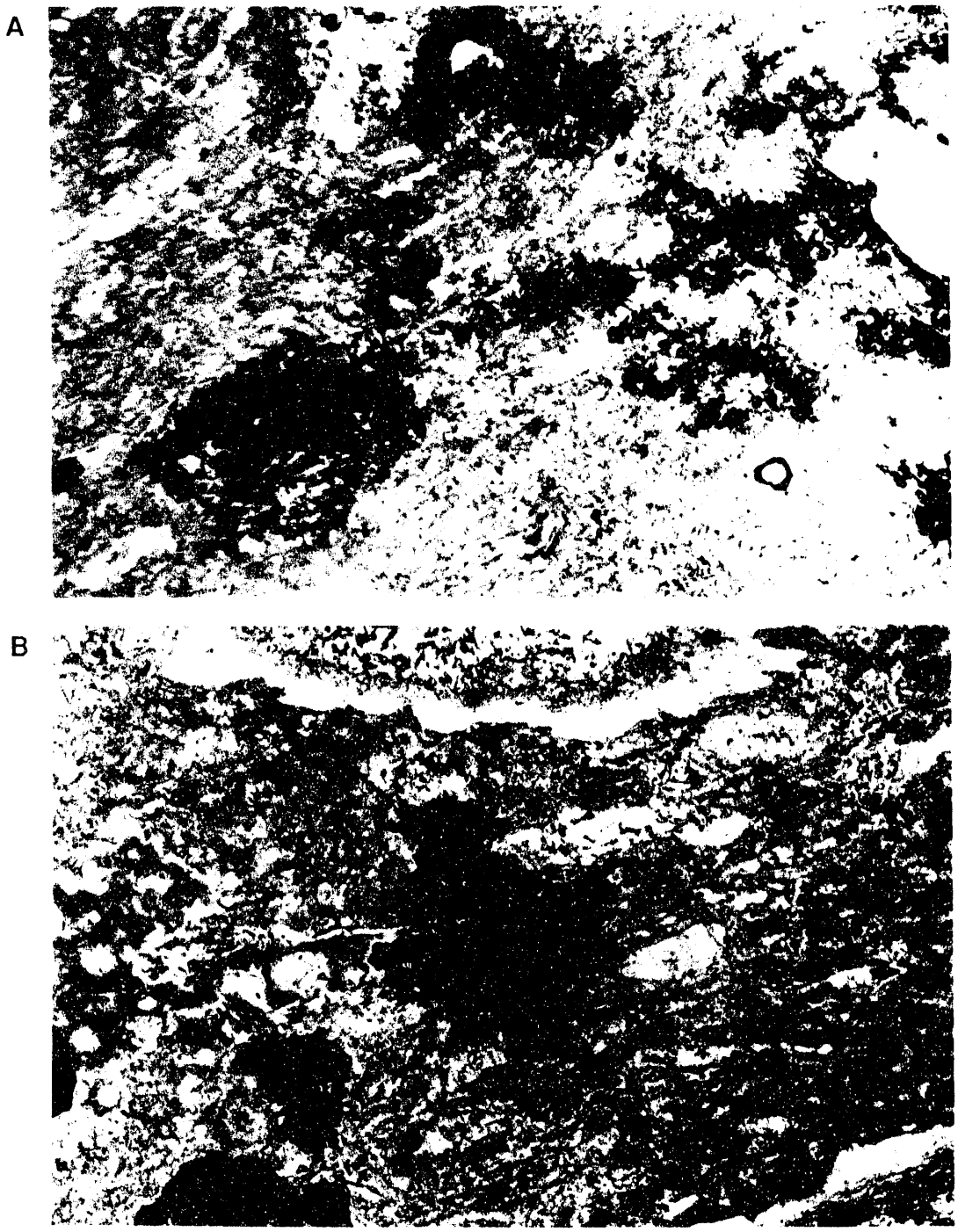

Fig. 4. Photomicrographs showing typical appearance of the common Mn-rich secondary clusters (dark blotches) in the welded tuff groundmass. Similar secondary phases fill partly open fracture trending diagonally from upper left corner in (A). Groundmass in (B) is darkened with finely disseminated hematite. Photos are 1.8 mm in length; plane-polarized light.

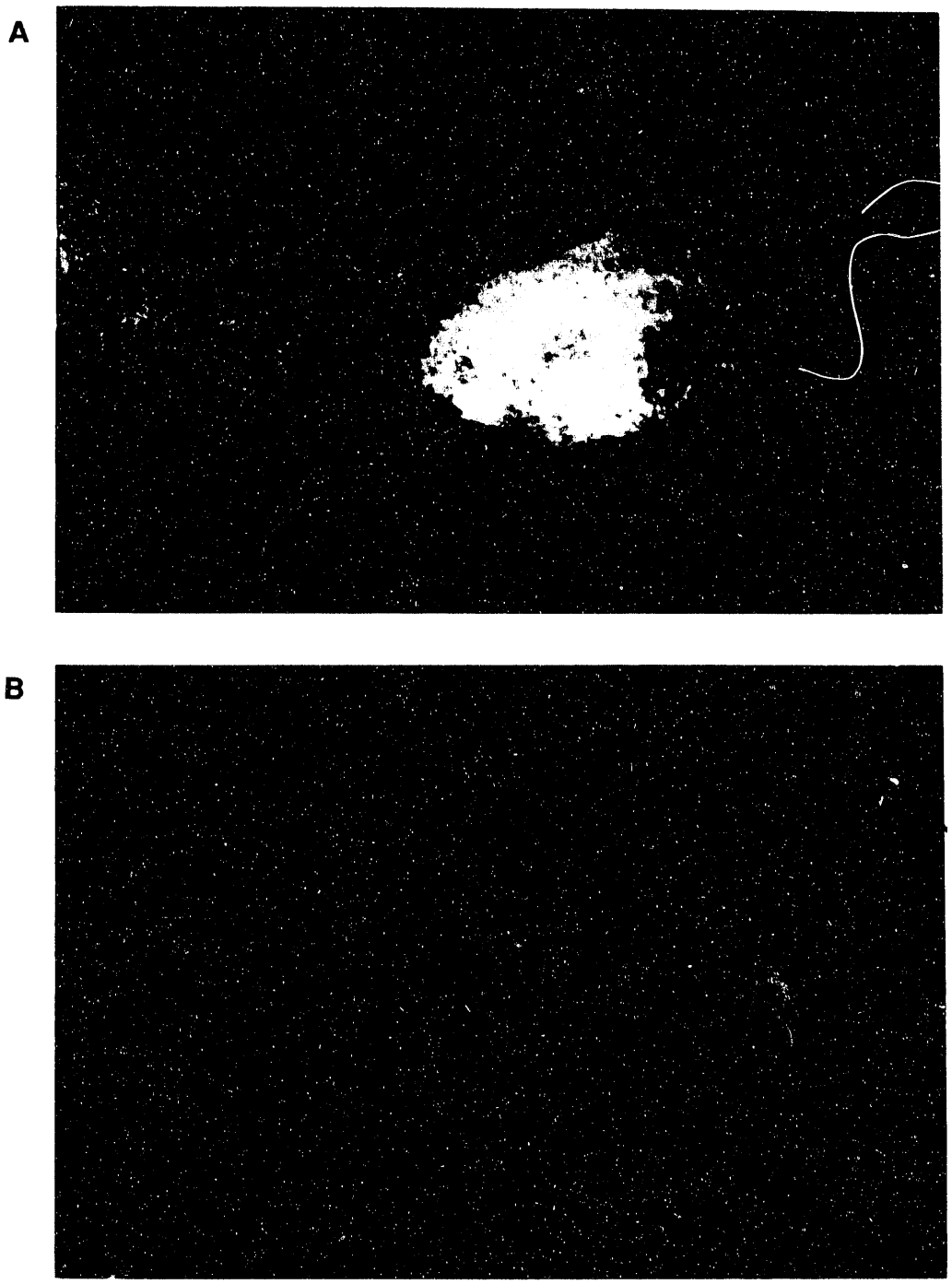

Fig. 5. (A): Back-scattered electron (BSE) image of composite opaque replacement grain, with adjacent Mn-rich opaque secondary phases in fracture (right side) and intergrown with groundmass (left).
(B): Corresponding fission track radiograph (photomicrograph, oblique light) showing U concentration of ~80 ppm in replacement grain, and lower concentration associated with the fracture and groundmass opaques.
Photos are both 1.3 mm in length.

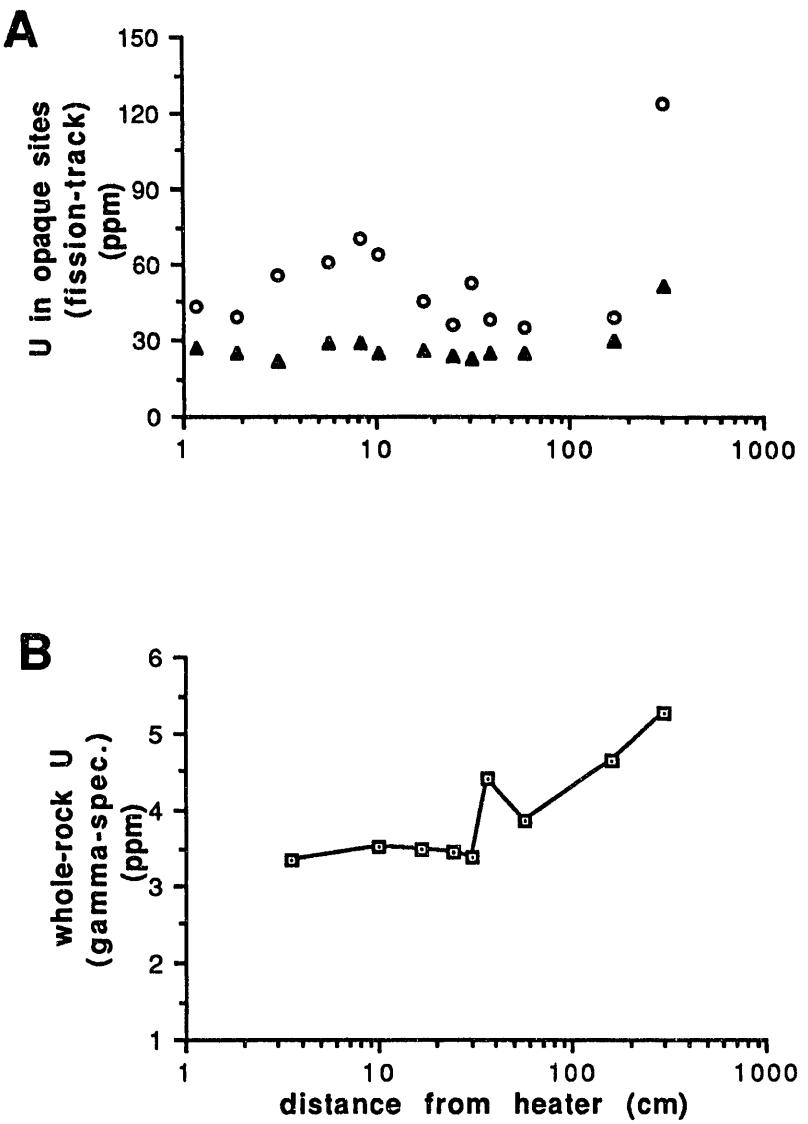

Fig. 6. Summary of microscopic (A) and whole-rock (B, from Fig. 3) distributions of U plotted against distance from heater edge. (A) shows data on opaque sites tabulated in Table 1: solid triangles depict secondary Mn-rich clusters; open circles combine data from primary and replaced-mafic opaques.

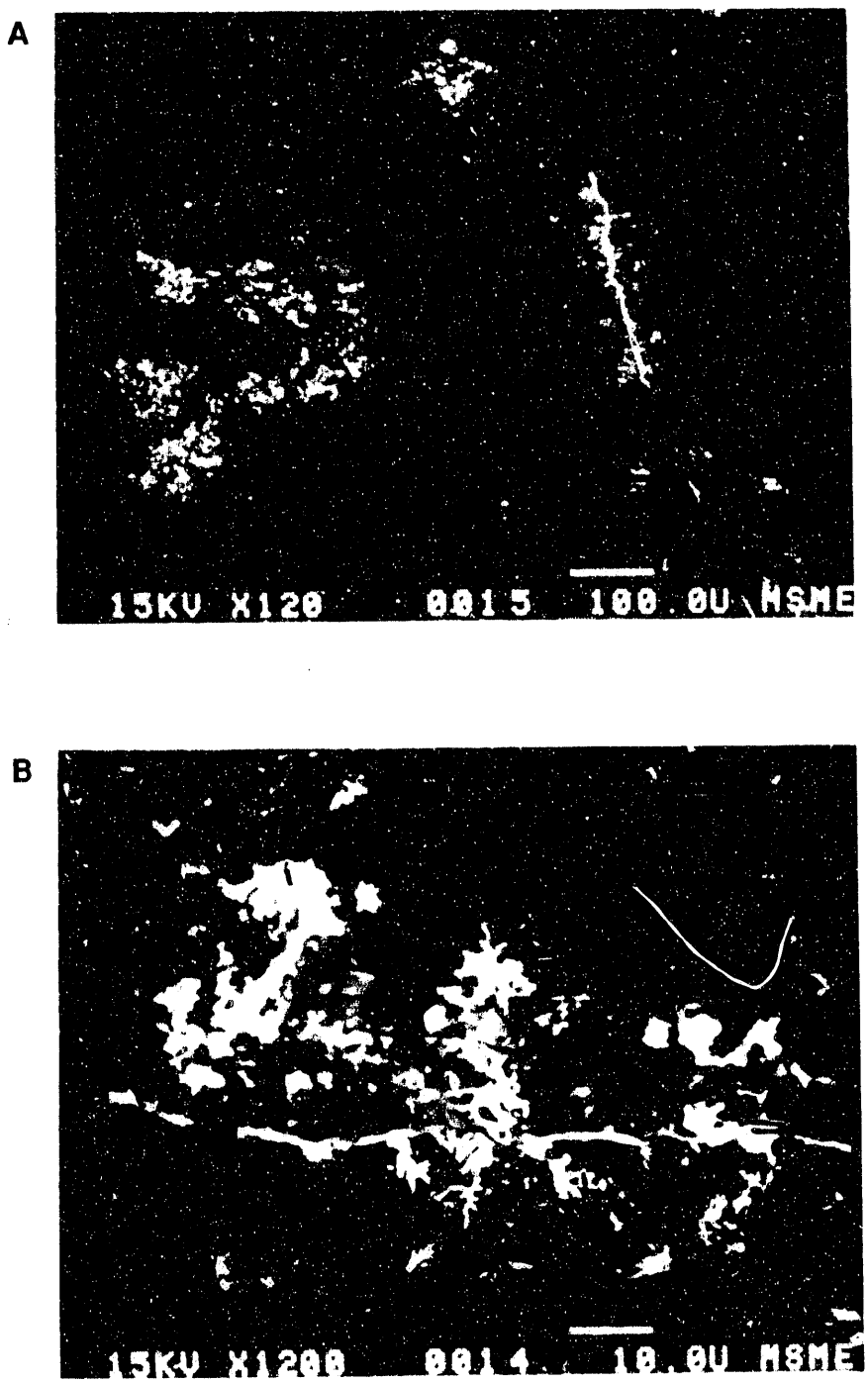

Fig. 7. BSE images of secondary Mn-rich phases in clusters intergrown in tuff groundmass, and partly filling fine fracture. (B) shows 10X magnification of adjacent part of fracture shown in (A). Bars are 100 μm (A), 10 μm (B).

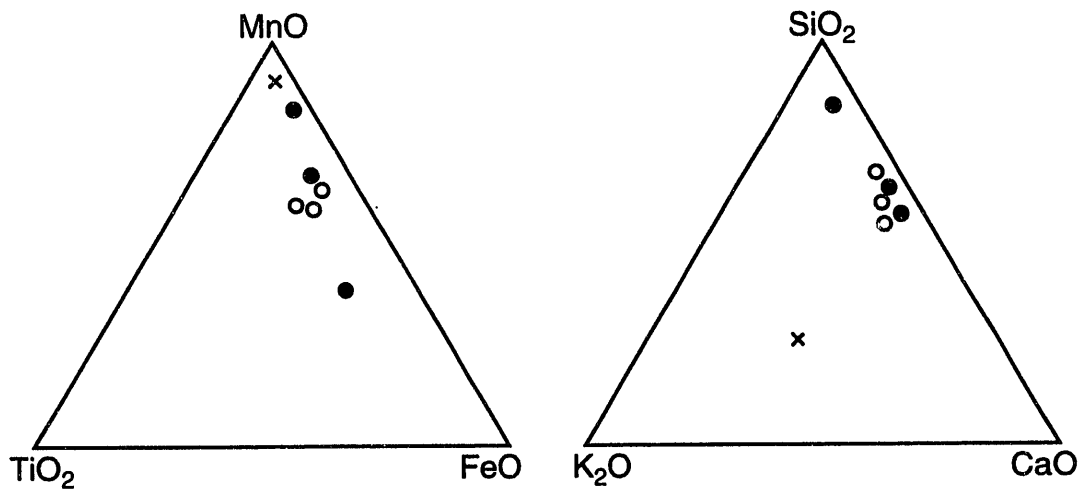

XBL 925-5267

Fig. 8. Ternary diagrams summarizing the data of Table 2:

- • common groundmass clusters
- o linings and acicular fillings of large pores
- x relatively thick fillings of fractures and micro-pores

A

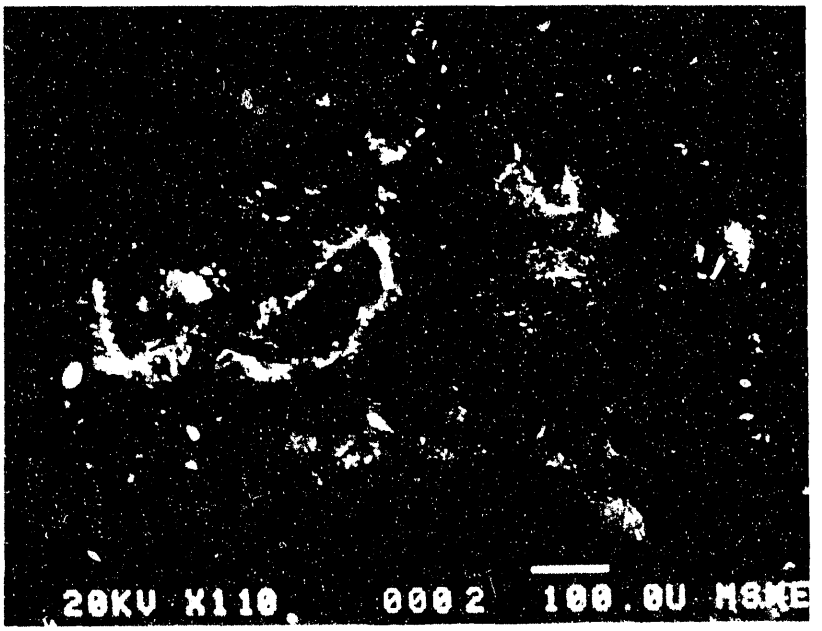

B

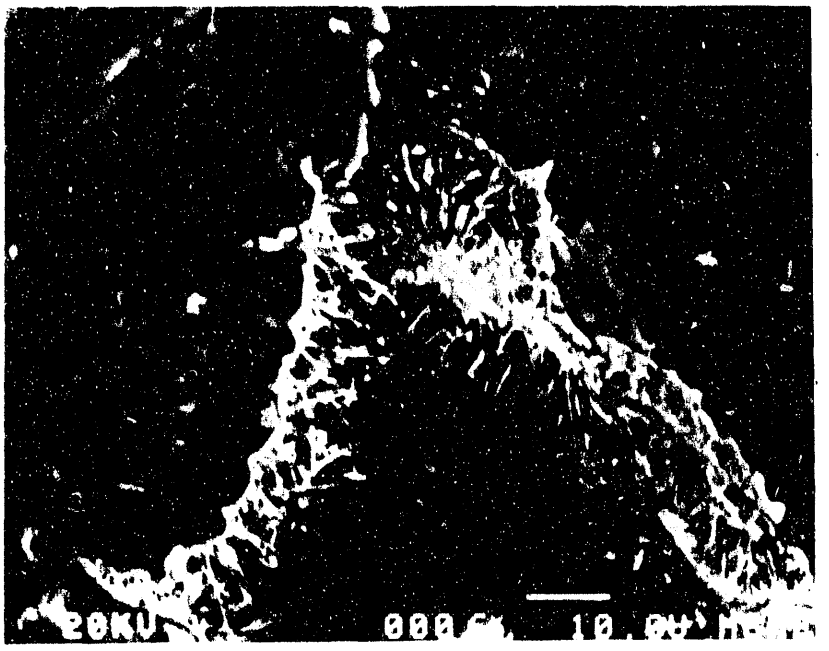

Fig. 9. BSE images of Mn phases partially lining large secondary pores in the tuff. Grains at bottom and upper right in (A) are alkali feldspar phenocrysts. (B) is magnified view of fine acicular pore-lining crystals; spherulitic devitrification texture is visible in tuff surrounding pore.
Bars are 100 μm (A), 10 μm (B).

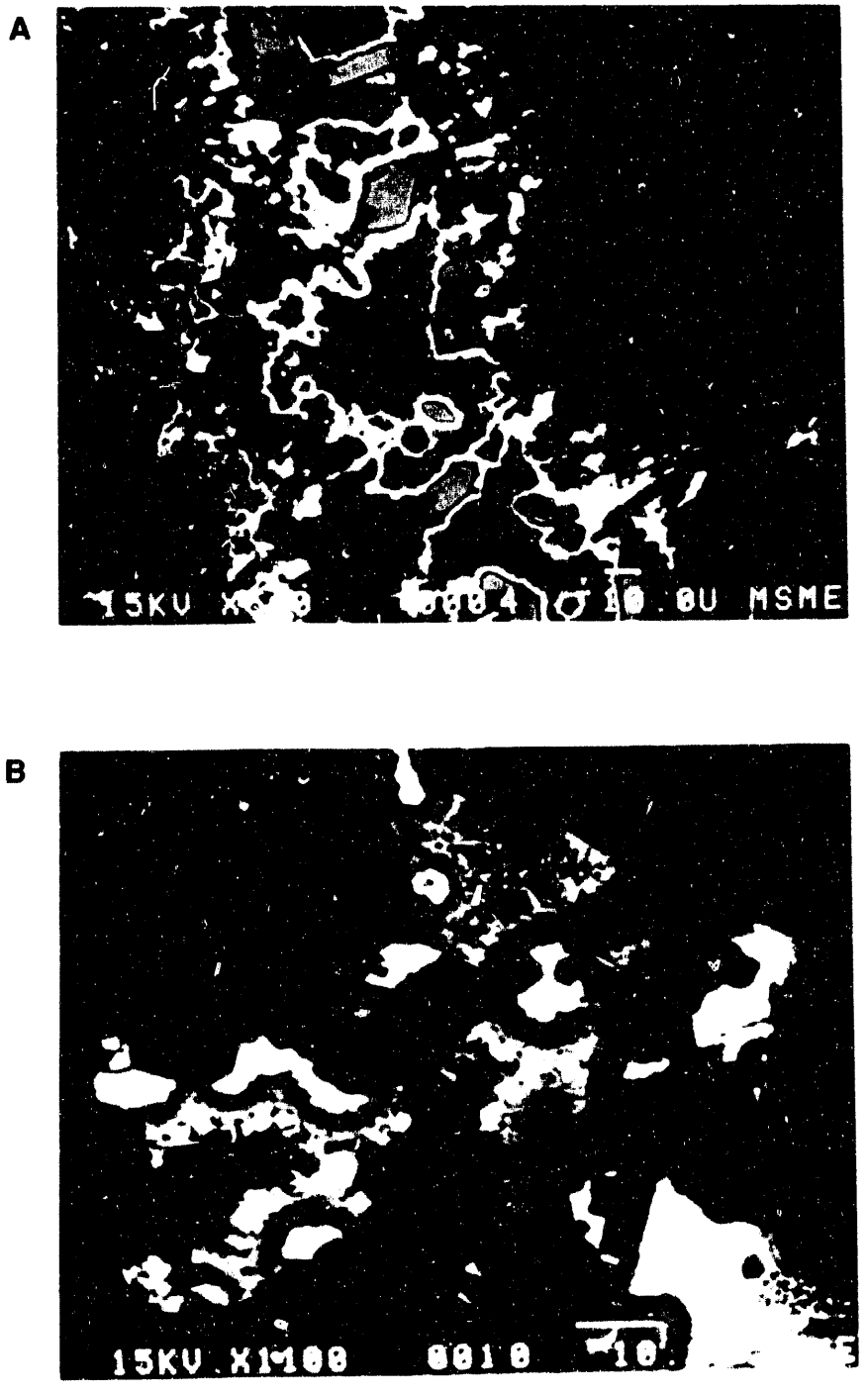

Fig. 10. Relatively thick pore-lining phases with high Mn concentrations. Acicular crystals also visible in (B). Bars are 10 μm.

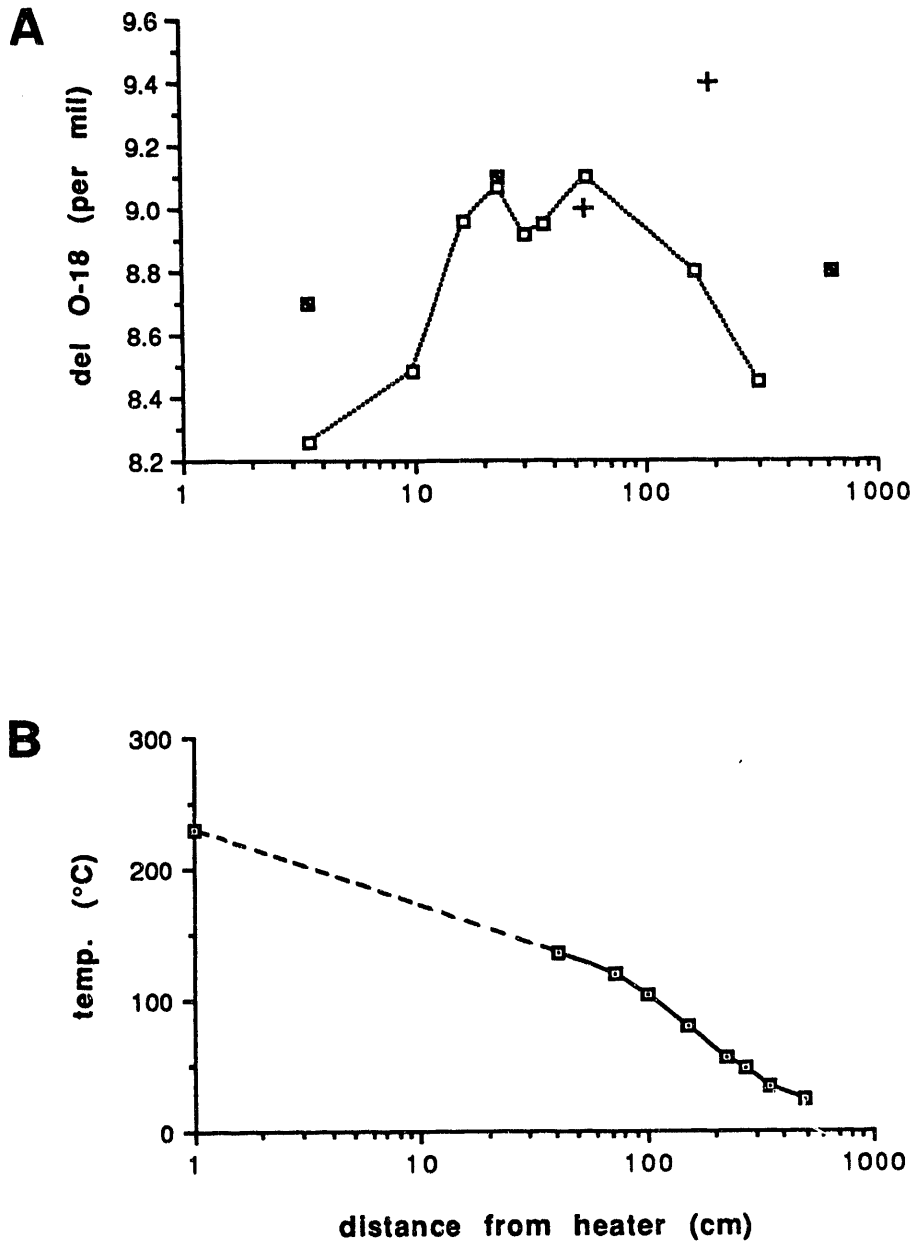

Fig. 11. Oxygen isotope ratios of tuff samples (A), compared with maximum heater test temperatures (B) from Fig. 3. Two sets of analyses are plotted: one set is P-1 drillback core samples, shown by dashed line and open squares (analyses by G.-M. Chang, LBL); other set includes 3 analyses of P-1 core (slashed squares), and 2 analyses of NE-2 unheated core (crosses) plotted at their approximate distances from the heater hole (analyses by Krueger Geochron, Inc.). Analytical uncertainty of isotopic ratios is approximately ±0.2 per mil.

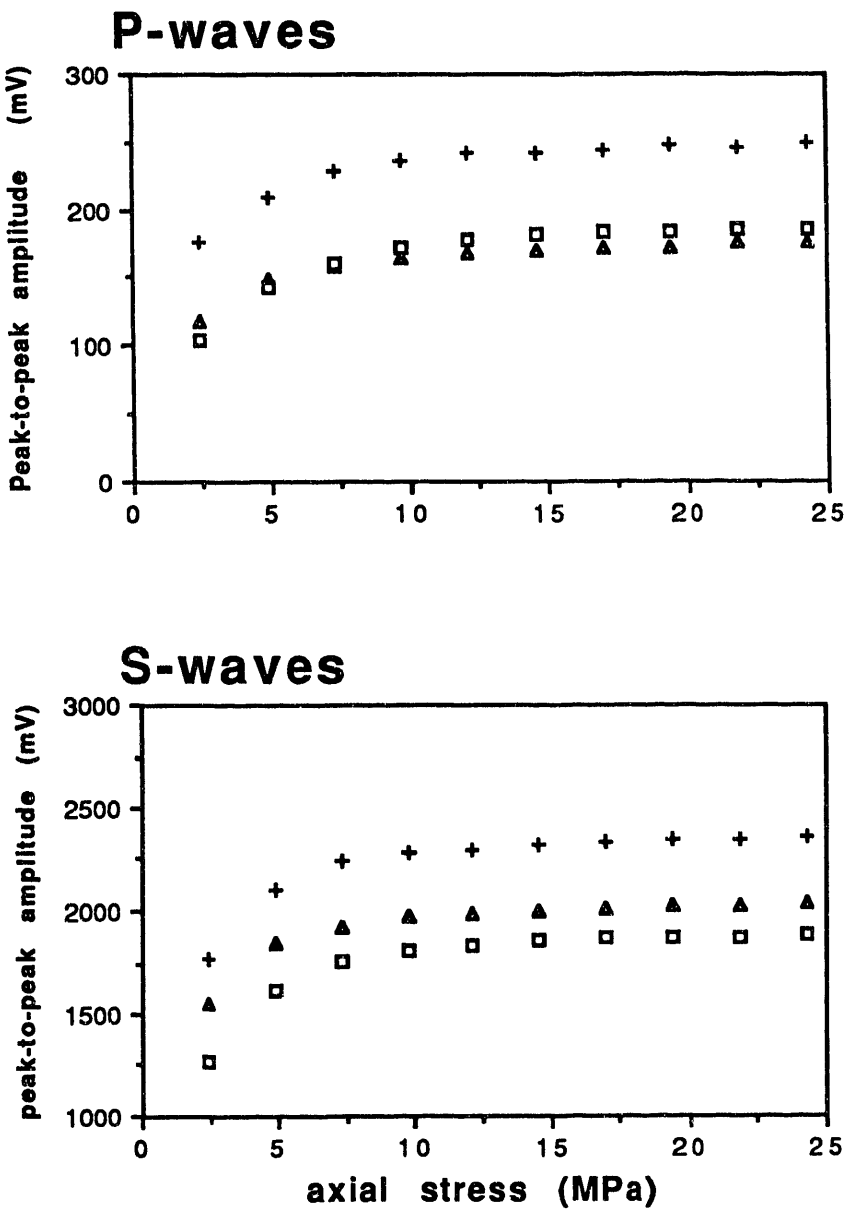

Fig. 12. Seismic amplitudes measured on 3 sub-cores drilled from P-1 drillback core. Distances of sub-core mid-points from heater edge are 3.5 cm (crosses), 17 cm (triangles), 30 cm (squares). Measurements performed by L. Myer and C. Nehay, LBL.

APPENDIX A

RADIOELEMENT CONTENTS OF CORE SAMPLES DETERMINED BY GAMMA SPECTROSCOPY

	bore-hole	mean distance from heater (cm)	#U (ppm)	Th (ppm)	K (%)
*	P1	3	3.33	16.47	4.31
	P1	10	3.51	16.21	4.31
	P1	17	3.49	16.61	4.40
	P1	24	3.45	16.60	4.24
	P1	30	3.38	16.65	4.34
	P1	37	4.42	20.70	5.71
	P1	56	3.87	19.60	5.26
	P1	163	4.64	20.40	5.27
	P1	300	5.26	20.00	4.96
**	NE-2	48	3.4	13.8	3.5
	NE-2	189	3.5	14.5	3.6
	NE-2	236	3.5	13.3	3.1
	NE-2	297	3.6	16.8	4.3
	NE-2	354	2.9	12.9	3.3
	NE-2	377	2.9	15.7	4.1
	NE-2	534	4.1	18.7	4.7
	NE-2	578	3.6	17.3	4.4
	NE-2	654	3.3	14.6	3.3

* P1: heated drillback core, drilled after heater test.
** NE-2: unheated core, drilled prior to heater emplacement.

To account for radon emanation, U concentrations should be increased by ~15% (as measured on two samples).

APPENDIX B

REPRESENTATIVE SEM X-RAY SPECTRA AND CORRESPONDING SEMIQUANTITATIVE ANALYSES (EDS) OF SECONDARY MN-RICH PHASES (SEE TABLE 2).

Vertical axes are counts (log scale); horizontal axes are x-ray energy, gridded in units of 1 KV.

Spectrum #:

(1) groundmass cluster, from Table 2, col. A. [20 KV, 90 sec.]
Small Ce L peak overlaps Ti K_β peak.

(2) groundmass cluster, from Table 2, col. B. [15 KV, 250 sec.]
Note Ce and P peaks (approx. 10% CeO_2 present).

(3) pore lining, from Table 2, col. D. [20KV, 90 sec.]

(4) fracture filling, from Table 2, col. G. [20KV, 90 sec.]
Small Zn peak from sample holder.

	(1)	(2)	(3)	(4)
MgO	n.a.	n.a.	2.6	n.a.
Al_2O_3	0.9	0.3	<0.5	<0.5
SiO_2	4.7	11.5	10.8	1.3
K_2O	0.7	0.7	0.7	3.5
CaO	6.0	5.6	2.0	2.4
TiO_2	3.1	3.4	12.7	3.3
MnO	72.6	47.0	49.9	86.8
FeO	12.0	11.8	19.8	2.7

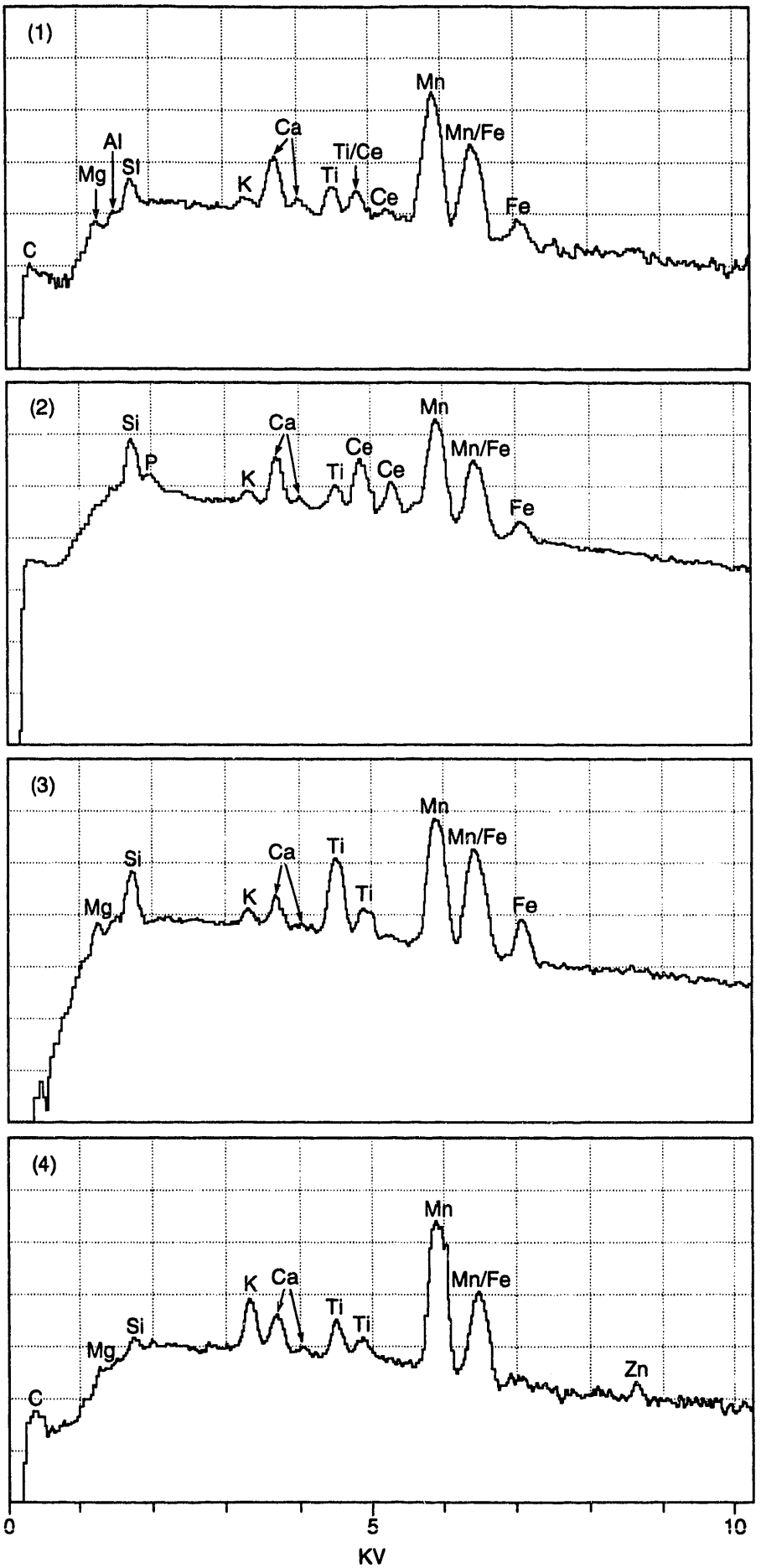
(1)
C
Mg
Al
Si
K
Ca
Ti
Ti/Ce
Ce
Mn
Mn/Fe
Fe
(2)
Si
P
K
Ca
Ti
Ce
Ce
Mn
Mn/Fe
Fe
(3)
Mg
Si
K
Ca
Ti
Ti
Mn
Mn/Fe
Fe
(4)
C
Mg
Si
K
Ca
Ti
Ti
Mn
Mn/Fe
Zn
0
5
10
KV

XBL 927-5734

APPENDIX C

OXYGEN ISOTOPE RATIOS

bore-hole	mean distance of core sample from heater (cm)	$\delta^{18}O$ (per mil) *LBL	**KEI
P1	3	8.26	8.7
P1	10	8.48	
P1	17	8.96	
P1	24	9.07	9.1
P1	30	8.92	
P1	37	8.95	
P1	56	9.10	
P1	163	8.80	
P1	300	8.45	
P1	640		8.8
NE-2	~55		8.9
NE-2	~55#		9.1
NE-2	~192		9.4

* Analyses by LBL Center for Isotope Geochemistry
** Analyses by Krueger Enterprises, Inc.

Duplicate analysis on separate aliquot.

Samples prepared from core by crushing, picking representative groundmass material, and sieving to obtain a 100-to-270 mesh separate.

APPENDIX D

1) SAMPLE CHARACTERISTICS AND SEISMIC VELOCITIES

mean distance from heater	3.5 cm	17 cm	30 cm
length (cm)	3.813	3.813	3.810
diameter (cm)	5.100	5.100	5.100
weight (g)	181.39	180.87	175.72
density (g/cm^3)	2.329	2.322	2.257
V_p (m/s)	2002	2002	1944
V_s (m/s)	1435	1455	1390
V_p/V_s	1.395	1.376	1.399

2) SEISMIC AMPLITUDES

	S-wave amplitudes (mV)			P-wave amplitudes (mV)		
stress (MPa)	3.5cm	17cm	30cm	3.5cm	17cm	30cm
2.43	1774	1556	1275	175.51	117.80	103.78
4.86	2104	1843	1621	209.84	149.37	143.15
7.29	2241	1925	1751	227.63	159.58	160.28
9.72	2287	1969	1812	236.62	165.37	172.75
12.15	2300	1987	1836	241.14	168.82	178.16
14.58	2324	2003	1857	242.07	170.11	181.56
17.01	2335	2016	1871	244.73	172.35	183.34
19.44	2340	2029	1878	247.40	173.16	183.31
21.87	2351	2032	1875	245.89	175.44	185.61
24.30	2364	2037	1885	248.92	175.44	186.40

END

DATE
FILMED
4 / 29 / 93